Carbon sequestration potential of Mg carbonate and silicate biomineralization in the presence of cyanobacterium Synechococcus

Céline Lamérand, Liudmila Shirokova, Pascale Bénézeth, Jean-Luc Rols, Oleg Pokrovsky

Chemical Geology

Carbon sequestration potential of Mg carbonate and silicate biomineralization in the presence of cyanobacterium Synechococcus

--Manuscript Draft--

Manuscript Number:	CHEMGE14674
Article Type:	Research paper
Keywords:	carbon, sequestration, biomass, carbonates, silicates, cyanobacteria, hydromagnesite.
Abstract:	Bacterially-induced sequestration of atmospheric CO 2 is at the forefront of geomicrobiological research due to high potential of this process in the mitigation of climate warming. Cyanobacteria have been known to form stromatolites for millions of years and could be used to enhance this process by sequestering carbon via the biomineralization of Mg and Ca carbonates. Currently, olivine (MgSiO 4) is considered as one of the most efficient silicate minerals suitable for CO 2 capture in the form of secondary Mg carbonates. However, the role of dissolved Si on the efficiency of biomineralization is not sufficiently well understood. The present study intended to reproduce in the laboratory the processes of biomineralization by Synechococcus sp. cyanobacteria extracted from modern stromatolites in a carbonate- and Mg-bearing medium containing various Si concentrations, in order to characterize the rates and stoichiometry of reactions as well as mineralogical nature of precipitates. The results demonstrated the dominant role of cyanobacterial metabolism in the precipitation of carbonate minerals by increasing the pH of the medium via photosynthesis and providing a template in the form of cell walls and their EPS for mineral nucleation. Transmission electron microscopy and other microscopic and spectroscopic observations and analyses identified magnesium carbonates and silicates, such as nesquehonite (MgCO 3 ·3H 2 O) and/or hydromagnesite (Mg 5 (CO 3) 4 (OH) 2 ·4(H 2 O) together with sepiolite (Mg 4 Si 6 O 15 (OH) 2 ·6H 2 O) as dominant precipitated minerals. Apparent inorganic C precipitation rates were not affected by the concentration of Mg and Si in the initial solution. However, the carbon sequestration potential was 20-40% higher in the presence of Si. Overall, the experimental approach developed in this study allows efficient reproduction of combined Mg hydroxy-carbonate and hydrous silicate precipitation under cyanobacterial activity and helps to constrain optimal conditions of cyanobacteria-induced CO 2 sequestration.

Graphical Abstract

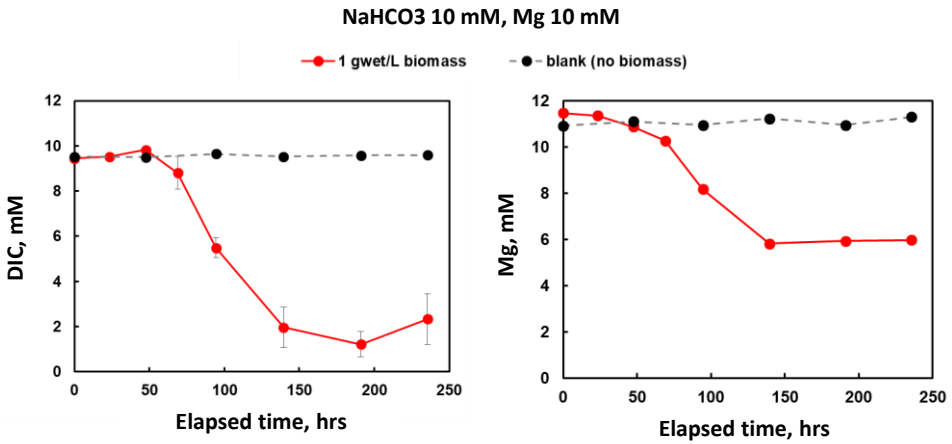

Simultaneaous decrease of DIC and Mg concentrations in the solution in presence of cyanobacteria

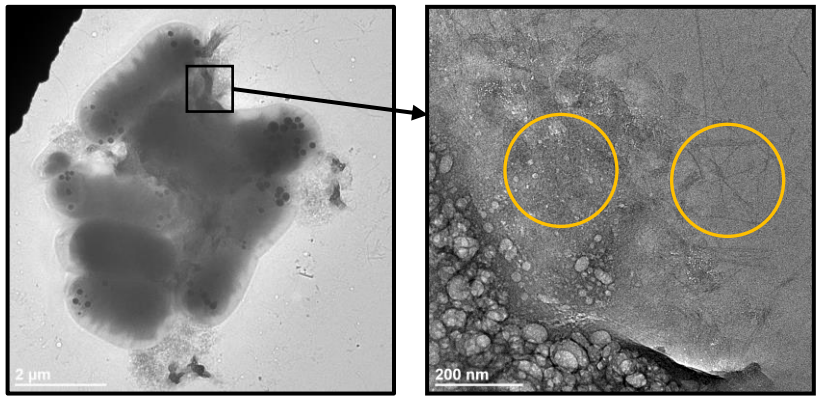

Formation of magnesian carbonates at the vicinity of cyanobacteria *Synechococcus* sp. cells

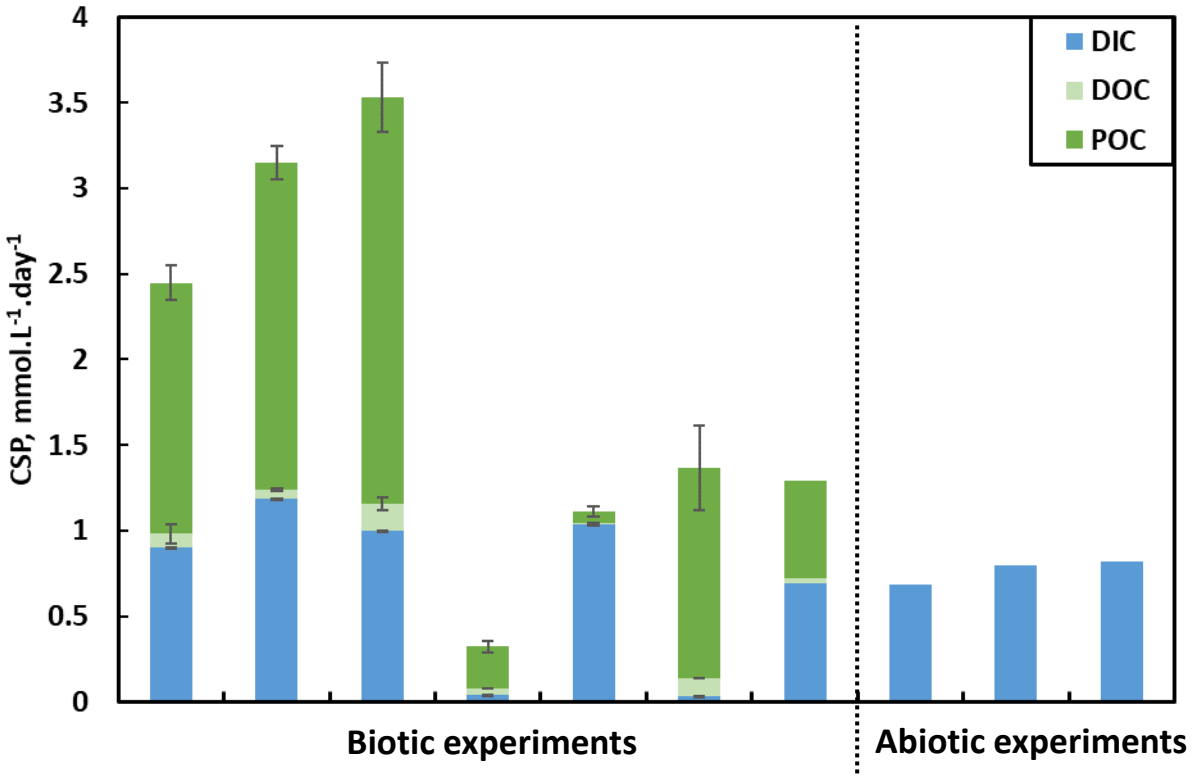

Carbon sequestered via the formation of Mg carbonate (DIC) and under organic forms in soluble organic matter (DOC) and in the cyanobacterial biomass (POC)

- Strong control of the cyanobacterial activity on hydrous Mg carbonate precipitation
- Increase in pH near the cells is the main driving factor of biomineralization
- Cyanobacterial surfaces and their EPS act as templates for carbonate mineral precipitation
- C was sequestered by particulate organic C and mineral form
- Aqueous Si increased carbon sequestration potential

Carbon sequestration potential of Mg carbonate and silicate biomineralization in the presence of cyanobacterium *Synechococcus*

Céline Lamérand[a], Liudmila S. Shirokova[a, b], Pascale Bénézeth[a], Jean-Luc Rols[c], Oleg S. Pokrovsky[a, d]*

[a] *Géosciences Environnement Toulouse, GET – CNRS – IRD – OMP – Université de Toulouse, 14, Avenue Edouard Belin, 31400 Toulouse, France*

[b] *N. Laverov Federal Center for Integrated Arctic Research of the Ural Branch of the Russian Academy of Sciences (FECIAR UrB RAS), Arkhangelsk, Russia*

[c] *Laboratoire écologie fonctionnelle et environnement, Université de Toulouse, CNRS, Toulouse INP, Université Toulouse 3 – Paul Sabatier (UPS), Toulouse, France*

[d] *BIO-GEO-CLIM Laboratory, Tomsk State University, Tomsk, Russia*

*Corresponding author email address: oleg.pokrovsky@get.omp.eu

Key-words: carbon, sequestration, biomass, carbonates, silicates, cyanobacteria, hydromagnesite.

Abstract

Bacterially-induced sequestration of atmospheric CO_2 is at the forefront of geomicrobiological research due to high potential of this process in the mitigation of climate warming. Cyanobacteria have been known to form stromatolites for millions of years and could be used to enhance this process by sequestering carbon via the biomineralization of Mg and Ca carbonates. Currently, olivine ($MgSiO_4$) is considered as one of the most efficient silicate minerals suitable for CO_2 capture in the form of secondary Mg carbonates. However, the role of dissolved Si on the efficiency of biomineralization is not sufficiently well understood. The present study intended to reproduce in the laboratory the processes of biomineralization by *Synechococcus* sp. cyanobacteria extracted from modern stromatolites in a carbonate- and Mg-bearing medium containing various Si concentrations, in order to characterize the rates and stoichiometry of reactions as well as mineralogical nature of precipitates. The results demonstrated the dominant role of cyanobacterial metabolism in the precipitation of carbonate minerals by increasing the pH of the medium via photosynthesis and providing a template in the form of cell walls and their EPS for mineral nucleation. Transmission electron microscopy and other microscopic and spectroscopic observations and analyses identified magnesium carbonates and silicates, such as nesquehonite ($MgCO_3 \cdot 3H_2O$) and/or hydromagnesite ($Mg_5(CO_3)_4(OH)_2 \cdot 4(H_2O)$ together with sepiolite ($Mg_4Si_6O_{15}(OH)_2 \cdot 6H_2O$) as dominant precipitated minerals. Apparent inorganic C precipitation rates were not affected by the concentration of Mg and Si in the initial solution. However, the carbon sequestration potential was 20-40% higher in the presence of Si. Overall, the experimental approach developed in this study allows efficient reproduction of combined Mg hydroxy-carbonate and hydrous silicate precipitation under cyanobacterial activity and helps to constrain optimal conditions of cyanobacteria-induced CO_2 sequestration.

1. Introduction

One of the considered options to decrease the rising CO_2 concentration in the atmosphere is to capture the CO_2 and store it into geological reservoirs (Matter *et al*., 2009; Matter and Kelemen, 2009; Sun *et al*., 2020). An alternative and more permanent solution is the mineralization of CO_2 into mafic and/or ultramafic rocks (peridotites, serpentinites) composed of silicates of magnesium, iron and calcium, which allows a thermodynamic stable and safe storage (Oelkers *et al*., 2008; Matter and Kelemen, 2009; Bénézeth *et al*., 2014). Indeed, CO_2 can react with these minerals producing Ca, Mg and Fe cations forming carbonated minerals, thus reproducing natural biogeochemical carbon (C) cycle of weathering and carbonate mineral precipitation.

Numerous experimental and field studies are devoted to the mechanisms of serpentinization and carbonatation of ultramafic rocks, all useful in the context of a possible industrial storage of CO_2 and its valorization (see Kelemen *et al*., 2011). In these studies, the forsteritic olivine $(Mg,Fe)_2SiO_4$ is generally used as representative mineral of these rocks because it plays an important role in the mechanisms of geological CO_2 sequestration via carbonatation, both in abiotic (Sissman *et al*., 2013; Peuble *et al*., 2015) and biotic (Power *et al*., 2009; Shirokova *et al*., 2013; Bundeleva *et al*., 2014; McCutcheon *et al*., 2014; Martinez *et al*., 2016) systems. Microroganisms are capable of C sequestration through mineral trapping via precipitation of dissolved CO_2, usually in the form of carbonate minerals such as $CaCO_3$ (Mitchell et al., 2010; Dhami et al., 2014; Pan et al., 2018; Zhu et al., 2015, 2018; Zhuang et al., 2018; Saneiyan et al., 2019; Naveed et al., 2020; He et al., 2022) thus providing durable carbon immobilization over a geological time scale (Pires et al., 2012).

Among different microorganisms, cyanobacteria play a central role in the bio-precipitation of carbonate minerals. Being modern representatives of the first living organisms on the Earth, these bacteria have been forming carbonated rocks, called stromatolites, in shallow marine or

lacustrine environments (a few dozen meters), the oldest of which situated in south-west Greenland are aged of 3.7 Ga (Nutman *et al*., 2016). The potential of calcifying cyanobacteria for geological CO_2 storage was demonstrated by Jansson and Northen (2010). Some studies showed the precipitation of magnesian carbonates following the dissolution of olivine in the presence of green algae (unknown consortium) (Power *et al.*, 2011), cyanobacteria *Synechococcus* sp. (Martinez *et al.*, 2016) or bacterial consortium (Lamerand *et al*., 2019). The precipitation of hydrated magnesian carbonates was accelerated in the presence of cyanobacteria *Gloeocapsa* sp., via the increase of pH in bicarbonate-bearing solutions under conditions similar to those of the natural environment (Mavromatis *et al.*, 2012). For example, in the alkaline Salda Lake (Turkey), cyanobacteria *Synechococcus* sp. form stromatolites composed of hydrated magnesian carbonates such as hydromagnesite ($Mg_5(CO_3)_4(OH)_2{\cdot}4H_2O$), by locally increasing the pH and providing the nucleation sites on the surface of cells, allowing the formation of minerals (Shirokova *et al.*, 2013). In this lake, underground springs enriched with Mg due to dissolution of peridotites at the lake watershed, form waters rich in Mg and Si (Shirokova *et al.*, 2012).

Most of laboratory experimental studies of the formation of Mg carbonate by cyanobacteria were performed with solely aqueous Mg and carbonate in solution, yet the biomineralization of Mg carbonate in the context of CO_2 storage occurs in Si-bearing environments. Therefore, a possible effect of the presence of aqueous Si on Mg carbonate biomineralization should be investigated. It can be anticipated that photosynthetic activity of bacteria in aqueous solutions containing Si and Mg could provoke the formation of both carbonates and magnesium silicates as it is reported from modern stromatolites occurrences (Pace *et al*., 2016; 2018). In natural settings, magnesian calcite and sepiolite ($Mg_4Si_6O_{15}(OH)_2{\cdot}6H_2O$) occur in lakes, subject to massive algae blooms (Barbiero *et al.*, 2002; 2008). Moreover, sepiolite was reported to form under controlled laboratory environment as a precursor of protodolomite (Balan *et al.*, 2018).

Despite numerous studies on Mg carbonate biomineralization via cyanobacteria, the processes leading to the formation of these minerals are not fully understood yet. Two main mechanisms of bio-induced precipitation are currently identified: (*i*) the increase of pH and saturation state of solution due to the photosynthetic activity of cyanobacteria (Lee *et al*., 2004; Plee *et al*., 2010 Ludwig *et al*., 2005) and (*ii*) mineral crystallization on exopolymeric substances (EPS) that could decrease the activation barrier via serving as nucleation centers (Dupraz *et al*., 2009). However, assessing the relative role of each of these mechanisms has not yet fully achieved.

The aims of this study were to 1) acquire new knowledge on the optimal conditions for massive precipitation of Mg carbonate and Mg silicate minerals in the context of CO_2 storage; 2) quantify the rates and characterize the nature of the precipitated solid phases, and 3) identify the mechanisms responsible for the biomineralization processes. For this, we conducted ~~different~~ laboratory experiments with *Synechococcus* sp. cyanobacterium, obtained from alkaline (pH > 9) Salda Lake (Turkey) using carbonate-bearing solution containing different concentrations of Mg and/or Si under different experimental settings, designed to distinguish the effect of solution supersaturation rise, cell surface sites and cell soluble exometabolites. We used a combination of physico-chemical, microscopic and spectroscopic techniques to characterize the formation of organo-mineral solid phases in order to produce a quantitative model of mineral formation in the system Mg - HCO_3 - Si - cyanobacteria at various physicochemical parameters of solution and to estimate the C sequestration potential of this system.

2. Material and methods

2.1 Bacterial strain

Cyanobacteria *Synechococcus* sp. PCC 7942 were isolated from the surface of stromatolites growing in the alkaline, $Mg(HCO_3)_2$-dominated Salda Lake (Turkey) and used previously in mineral carbonation experiments in pure culture (Shirokova *et al*., 2013). They were cultured in BG-11 (Sigma-Aldrich C3061) nutrient solution under air bubbling and continuous light to insure most efficient development (Stanier *et al*., 1979). Before the inoculation of batch reactors, cells were rinsed twice in appropriate fresh culture media or sterile 0.1 M NaCl solution using centrifugation (~500 mL of solution for 1 g of wet biomass) to remove, as possible, the adsorbed ions and cell exudates from the surface.

2.2 Aqueous solutions

The precipitation of secondary Mg-carbonate and Mg-silicate minerals in the presence of cyanobacteria *Synechococcus* sp. was studied in aqueous solutions of 10 mM $NaHCO_3$ enriched or not with Mg and Si. Aqueous silica was added from a Na_2SiO_3 concentrated solution and Mg was added from a $MgCl_2$ concentrated solution. Various control experiments were performed as similar composition of aqueous solution. The composition of experimental fluids is listed in **Table 1**.

2.3 Experimental setup

Experimental setup was aimed at testing separately the effect of Mg, HCO3, Si concentration, pH of the aqueous solution, cell photosynthesis, EPS, and the presence of cell surfaces as templates for mineral crystallization. All the experiments were run in duplicates and included: *i*) cyanobacterial suspension in 500 mL polycarbonate Erlenmeyer flasks closed with sterile porous caps (Bio-Silico®) which allowed free atmospheric air exchange (experiments Mg3, SiMg3, SiMg), *ii*) cyanobacteria enclosed into a dialysis bag (pore size 6-8 kDa, ~2 nm) placed in a glass beaker also in free exchange with atmosphere (experiment DSM, **Fig. 1A**), *iii*)

dialysis bags (6-8 kDa, ~2 nm) containing a solution of 10 mM $NaHCO_3$ and 10 mM of Mg were placed into a polycarbonate jar filled up with the same solution in which 1 g_{wet} L^{-1} of cyanobacteria *Synechococcus* sp. was added (experiment SD, **Fig. 1B**), *iv*) cyanobacterial suspension without BG-11 nutrient under light (experiment BSM), *v*) cyanobacterial suspension in the darkness (aerated bottles wrapped in aluminum foil; experiment CSM), and *vi*) abiotic experiments where NaOH was added to reproduce the increase of pH due to photosynthesis in biotic experiments (experiments AMg3, ASiMg3, ASiMg). All experiments were run at 25±1°C with an orbital shaker (for DSM) or under magnetic stirring (all other experiments). Biotic experiments were carried out under cool fluorescent lights of constant 2500 lux (~40 $\mu mol.m^{-2}.s^{-1}$, in duplicates and with abiotic controls. A 10% diluted BG-11 solution (freshwater cyanobacteria nutrient solution) was used as a nutrient source for bacteria except for BSM experiment. All manipulations were performed under sterile conditions in a laminar flow hood class A100. .

2.4 Sampling procedure

Samples were taken daily during the first week and then every 2-3 days in order to follow the evolution of different microbiologic and physicochemical parameters (biomass, pH, alkalinity, concentrations in Mg, Si and dissolved organic carbon (DOC)) and to characterize eventual precipitation of secondary minerals. An aliquot of 20 mL was taken during vigorous stirring to maintain the homogeneity of the suspension, and subdivided into several parts. The first 5 mL were used to measure the cyanobacterial concentration and the pH. The remaining 15 mL were centrifuged (3500 g, 30 min) and the supernatant was filtered (0.45 µm). A part of this filtrate was used to analyze the alkalinity (Alk), Si and DOC concentrations. The other part was acidified with HNO_3 to measure Mg^{2+} concentration. The filtrates were preserved at 4°C pending analyzes.

2.5 Chemical analyzes

Cyanobacterial biomass was calculated from optical density of suspension at 680 nm (OD_{680nm}), using a Helios Epsilon spectrophotometer. The conversion factor from OD_{680nm} to dry biomass (g_{dry}/L) was equal to 0.519 and the ratio wet:dry biomass was 8±0.5. The pH was measured with a combination pH-electrode (Schott Geräte H62), with an uncertainty of 0.01 units. NIST buffers (pH = 4.00, 6.88, 9.22 at 25°C) were used for the calibration of the electrode. The total silica concentration was measured by colorimetry with the molybdate blue method using a colorimetric chain Technicon Autoanalyzer II, with an uncertainty of 2% and a detection limit of 3×10^{-7} M. Dissolved inorganic carbon (DIC) was calculated from pH and alkalinity, which was determined by a standard HCl titration using an automatic Schott TitroLine alpha plus titrator, with an uncertainty of 1% and a detection limit of 5×10^{-5} M. Magnesium concentration was measured by flame atomic absorption spectroscopy using a Perkin Elmer AAnalyst 400 with an uncertainty of 1% and a detection limit of 1×10^{-7} M. The DOC was determined using a Shimadzu TOC-V_{CSN} analyzer with an uncertainty of 5% and a detection limit of 0.1 mg C_{org} L^{-1}.

The saturation indices were calculated using PHREEQC geochemical code (Parkhurst and Appelo, 1999), with its llnl.dat database modified to consider new equilibrium constants in the Ca-Mg-CO_2-H_2O system from Palmer and Wesolowski (1997), Millero *et al*. (2007), Bénézeth *et al*. (2011), Stefánsson *et al*. (2013; 2014), Gautier *et al*. (2014), and Harrison *et al*. (2019).

2.6 Microscopic analyzes

For Transmission Electron Microscopy (TEM) observations, samples were prepared in three different ways. The first method included aliquots of bacteria + precipitated mineral

suspension were centrifuged (30 min, 1000 rpm) and the organic matter was removed from the solid phase by treating them in aqueous 10% H_2O_2 overnight. The remaining solids were rinsed three times with MilliQ® water, freeze-dried at -50°C, and deposited on carbon-coated copper grids. The second method used a drop of fresh suspension (~1 g_{wet} L^{-1}) was deposited on a carbon-coated copper grid. Finally, the third method involved ultrathin slices for TEM analyses which were prepared as following: freshly sampled cells and precipitated minerals were fixed with 2.5% glutaraldehyde / 2% paraformaldehyde in 0.1 M cacodylate buffer (pH = 7.2) at ambient temperature for 1.5 h, then washed three times with 0.1 M cacodylate, and subsequently soaked in 1% osmium tetroxide at ambient temperature for 1 hour and washed three times with 0.1 M cacodylate. Supernatant was discarded and pellets were embedded in agarose, then samples were subjected to stepwise ethanol dehydration (15 min at 25, 50, 70 and 90% ethanol at ambient temperature, and 3 x 30 min at 100% dry ethanol). Samples were then embedded in epon and 80 nm thick ultrathin sections were prepared with a Leica UCT ultramicrotome. Ultramicrocuts were mounted on Cu formvar-carbon grids, and electron stained with uranyl and lead citrate. Grids were characterized using a JEOL JEM-2100F TEM coupled with an SDD Brucker EDS analyzer.

3. Results

3.1 Aqueous solution evolution in the presence of cyanobacteria

Results of experiments with a monoculture of cyanobacteria *Synechococcus* sp. in a 10 mM $NaHCO_3$ solution with various Mg and Si concentrations are presented in **Fig. 2A** (10 mM Mg), **2B** (10 mM Mg and 0.4 mM Si) and **2C** (5 mM Mg and 0.3 mM Si). In experiments with 10 mM of Mg, the pH increased from 9 to 11.3 during the first 80 hours, then it became stable until the end of experiments (**Figs. 2A-B**). Note that the pH and the concentration of DIC, Mg and Si were stable in blanks. The DIC was stable at 10 mM during the first 50 hours then

decreased by 90-95% during the next 150 hours. The Mg concentration slightly decreased (~10%) during the first 50 hours, and then further decreased two-folds during the following 100 hours. In the experiment without Si, the Mg concentration remained stable until the end of the experiment (**Fig. 2A**), whereas it still decreased from 6 mM to 4 mM in the presence of Si (**Fig. 2B**). At 0.4 mM of initial Si, the Si concentration decreased by 99% during the first 150 hours and then remained stable (**Fig. 2B**). The simultaneous sharp decrease of DIC, Mg and Si (when present) concentrations at high pH values suggested the precipitation of magnesium carbonates and/or silicates.

In experiments with 5 mM of Mg and 0.3 mM of Si, the evolution of different parameters was similar to the experiments previously described, with an increase of pH from 9 to 11.3 during the first 100 hours, and a loss of 90% of DIC and 98% of Mg and Si between 100 and 240 hours (**Fig. 2C**).

Considering the decrease of DIC, Mg and Si concentrations and the pH evolution in the course of experiments, the saturation indices (SI) calculated with PHREEQC indicated a possibility of precipitation of Mg carbonate and silicate minerals: artinite, hydromagnesite, brucite and sepiolite (**Figs. 2A-C).** The SI values of artinite, brucite and hydromagnesite were negative at the beginning of experiments and increased to reach a maximum of 3, 2 and 5, respectively, between 70 and 100 hours; subsequent decrease of SI indicated a possible formation of these minerals. The SI of nesquehonite was negative in all experiments. In experiments where Si was added (**Figs. 2B-C**), the SI of sepiolite was positive from the beginning until the end of experiments, and a decrease of Si after about 100 hours of experiment indicated a possible precipitation of this mineral.

In experiments without 10% BG-11 nutrient medium (BSM), the pH increased from 8.5 to 9.6 between 0 and 96 hours and remained stable until the end of the experiment (**Fig. 3A**). A lack of nutrients in the solution did not allow the cyanobacteria to metabolize and produce

sufficiently high pH. Consequently, no precipitation was observed: the concentration of DIC remained stable at 10 mM. The Mg concentration decreased from 12 to 9.8 mM, which could be due to its uptake and adsorption by cyanobacteria for nutrient requirement.

During experiments in the darkness (CSM), cyanobacteria did not photosynthesize; thus, their biomass and solution pH remained stable. A decrease of Mg concentrations during the first 96 hours may indicate a consumption of this potential nutrient by cyanobacteria (**Fig. 3B**). Increasing artificially the pH to 10 led to a decrease of DIC concentrations from 10 to 4 mM between 96 and 200 hours. Further increase in pH to the value of 10.6 led to a rapid decrease of Mg concentration (from 9.8 to 7.2 mM in an hour). Thus, a concomitant decrease of both DIC and Mg concentrations indicated the formation of Mg carbonate in the solution.

During experiments with cyanobacteria which were confined within a dialysis bag (DSM), the photosynthetic activity induced an increase in pH inside and outside of the dialysis bags from 8.9 to 10 over the first 380 hours of the experiment (**Fig. 3C**). Magnesium concentration slightly decreased from 13 to 11.5 mM during the first 24 hours and then remained stable. The DIC concentration was stable at 10 mM during full duration of the experiment. Note that ion concentrations inside the dialysis bag were measured at the beginning and the end of the experiments and were similar to those outside of the bag (not shown). Even though pH increased, no precipitation was observed in these experiments.

When cyanobacteria were placed outside of the dialysis bag (SD), the pH value and Mg concentration were similar in and out of the bag, while the DIC was equilibrated between two compartments at 10 mM after 250 hours of exposure (**Fig. 3D**). The pH increased from 8 to 11 in 400 hours, the Mg concentration decreased from 12 to 8 mM between 0 and 300 hours of experiment, and the DIC concentration decreased from 9.8 to 4 mM between 250 and 410 hours of experiment, when pH reached a value of 10.5, thus indicating the precipitation of Mg carbonate. The formation of this phase was clearly observed outside the dialysis bag in the form

of a mixture of the mineral deposit and cyanobacterial biomass at the bottom of the reactor and on its walls (**Fig. S1A**), as well as on the external surface of the dialysis bags (**Figs. S1B-C**).

3.2 Microscopic and spectroscopic characterization of solid phases formed during the biotic experiments

In order to reveal the relationship between cyanobacterial cells and precipitated mineral phase(s), the experimental suspension was examined with transmission electronic microscopy (TEM) after one and two weeks of experiment with 10 mM of Mg and 0.4 mM of Si in the initial solution (**Figs. 4 and 5**). After first week, a solid fibrous phase was visible around the cyanobacteria cells (**Fig. 4A**, top and bottom right). Thin, hair-like needles were detectable in the immediate vicinity of the cell (shown at the bottom of **Fig. 4A**). The observation in dark field using a diaphragm allowed to distinguish the crystalline particles, appearing in bright white on **Fig. 4B**, from the amorphous phase appearing in grey on the same figure. The Fast Fourier Transform (FFT) pattern confirmed the presence of a crystalline phase (**Fig. 4C**) particularly in the zone encircled in red on **Fig. 4B**, where the quantity of white particles was the highest. After two weeks of experiments, cyanobacteria were surrounded by some solid phase (**Fig. 5A**). Near the cells, nanometric white particles were clearly detectable (encircled in the left, **Fig. 5B)**. At some distance from the cells (100-200 nm), thin needles were present (**Fig. 5B**, in the right circle). At the same time, at the end of experiment, solid fibrous phase was not detectable anymore. The FFT pattern indicated the presence of a crystalline phase in the spots where the largest amount of white nanoparticles was concentrated (**Fig. 5C**). An energy dispersive X-ray spectrometry (EDS) analysis allowed the determination of the chemical composition of the crystalline phases after one and two weeks of experiment (**Figs 4D and 5D, respectively**). These phases contained mostly magnesium (~ 40%), oxygen (~ 35%) and carbon (7 to 17%). Hence the crystalized phases could be hydrous magnesian carbonates. In the sample

retrieved after one week of reaction, silicon was also present (12%), which could correspond to a magnesian silicate such as sepiolite. No crystalline phase was detected within the needles. However, the needles could be too thin (i.e., less than 10 nm wide) to reveal the nature of constituent minerals.

The TEM observations of the experimental suspension collected outside the dialysis bags (experiment SD) revealed a crystalline phase near the *Synechococcus* cells (**Figs. 6A-B**). According to the EDS analysis realized in the red circle on **Fig. 6B**, this phase contained mostly carbon (47%), magnesium (38%) and oxygen (13%) (**Fig. 6D**), which could indicate the presence of hydrous Mg carbonate. In the sample collected from the experiment in the darkness (CSM), a crystallized precipitated phase composed of Mg, C and O was also present but no cells were visible, and there was only some residual organic matter from the bacterial cells which were present at the beginning of the experiment (**Fig. S2**).

The FFT patterns obtained from the crystalline phases after one and two weeks of experiments (**Figs. 4C and 5C**, respectively) and from the experiment SD in the dialysis bag (**Fig. 6C**) yielded an average lattice thickness of 0.153 nm, which is similar to the major reflection (d_{101}, 100% intensity) of nesquehonite, a magnesian carbonate ($MgCO_3 \bullet 3H_2O$), and one of the major reflection (d_{110}, 73% intensity) of hydromagnesite ($Mg_5(CO_3)_4(OH)_2 \bullet 4\ H_2O$).

In order to observe the intra- and extra-cellular precipitation, a cross-sectional TEM observation of organo-mineral aggregates formed in SiMg3 experiment during 2 weeks of incubation was also realized (**Fig. 7**). A longitudinal section of the cyanobacteria *Synechococcus* sp. (**Fig. 7A**) revealed a black photosynthetic membrane and dark spherical formations corresponding to intracellular phosphate globules consistent with previous observations (Lamérand *et al*., 2020). Inside the cells, white formations a few nm in size were detected (**Fig. 7B**). Some mineral solid phase was also present outside the cells (**Fig. 7C,** black formations), in which an EDS analysis revealed the presence of Mg and Si. Finally, some

filaments were visible on the cell membrane (**Fig. 7B**); however, they were too thin to be characterized by EDS analysis. These could be EPS released by the bacteria during their metabolic activity.

3.3 Abiotic experiments

In abiotic experiments, we artificially increased the pH via progressive addition of NaOH to approximate a temporal pattern of the pH rise due to photosynthesis in the biotic experiments. The precipitation of hydrous Mg-carbonate and Mg-silicate occurred when the pH reached the value of ~10.3, accompanied by a simultaneous decrease of DIC, Mg and Si (when present) concentrations in solution (**Figs. S3 A-C**).

SEM observations of the mineral formed during the experiment showed the presence of rosette-like crystals in the experiment AMg3 (**Figs. 8A-B**), similar to Mg carbonate hydromagnesite and dypingite. These crystals were partially visible in the experiment ASiMg3 (**Figs. 8C-D**) together with a granular, probably amorphous phase, which was the only one visible in the ASiMg experiment (**Figs. 8E-F**). These observations were confirmed by XRD analysis, which showed a mixture of hydromagnesite and dypingite in the sample from AMg3 experiment (**Fig. S4**), whereas no crystalline phase was detected in the samples from Si-bearing abiotic experiments (ASiMg and ASiMg3, not shown).

3.4 Rates of precipitation

Apparent rates of Mg, Si and DIC concentrations decrease (mmol L^{-1} day^{-1}) were calculated for the stage of maximum precipitation, according to the following equations:

$$R_{Mg} = \frac{d[Mg]}{dt}, R_{Si} = \frac{d[Si]}{dt}, R_{DIC} = \frac{d[DIC]}{dt}$$

These rates are listed in **Table 2**. In most experiments, a higher initial Mg concentration led to a faster decrease of Mg and DIC concentrations. Under the same initial conditions, the rate of DIC decrease was similar for abiotic and biotic experiments. In the abiotic experiments, a decrease of Mg concentration was slightly slower (0.62-0.96 mmol L^{-1} day^{-1} compared to 0.76-1.5 mmol $L^{-1}day^{-1}$ in the biotic experiments). This difference could be explained by intracellular consumption and/or surface adsorption of Mg by cyanobacteria in biotic experiments in addition of Mg precipitation, while in the abiotic experiments only the precipitation occurred. The magnitude of Si concentration decrease was similar regardless the initial Si concentration but the apparent rate was faster in abiotic experiments compared to biotic experiments (~0.2 mmol L^{-1} day^{-1} and ~0.1 mmol L^{-1} day^{-1}, respectively).

4. Discussion

4.1. Precipitation of secondary minerals: rates and identity of secondary phases

Distinct precipitation of secondary minerals was observed in a biotic (1 g_{wet} L^{-1} of bacterial biomass) carbonate-bearing environment with different concentrations in Mg and Si. Fast and simultaneous decrease of the Mg and Si (when present) concentrations in biotic experiments (1 g_{wet} L^{-1} of biomass, **Fig. 2**) indicated the precipitation of magnesian carbonates and/or silicates, highlighting the governing role of cyanobacteria in the secondary phase formation. Indeed, during the photosynthesis, cyanobacteria increased the pH above 10.3 (**Fig. 2**), thus rising significantly the supersaturation degree of solution with respect to artinite, hydromagnesite, brucite and sepiolite. This induced the precipitation of phases which could not be formed at lower pH values.

The observation by TEM coupled with EDS analysis highlighted the presence of crystalline hydrous magnesian carbonate phases in the vicinity of bacterial cells (**Figs. 4-7**). The FFT patterns allowed identifying these minerals as nesquehonite and/or hydromagnesite,

whereas temporal evolution of saturation indices during experiments indicated the possible precipitation of hydromagnesite but not nesquehonite. However, at the surface of cells, the pH is known to be much higher than that measured in the bulk solution (Revsbech *et al*., 1983, Dupraz *et al*., 2009). Although this is generally applied to cyanobacterial biofilms, unicellular photosynthesizing plankton is also likely to exhibit a sizable pH gradient suitable for precipitation of carbonate minerals (Pokrovsky and Savenko, 1995). Therefore, cyanobacterial photosynthesis could have induced a much higher local supersaturations leading to the crystallization of nesquehonite, which could have evolved over time into hydromagnesite as it is known from other biotic and abiotic experiments. Generally, nesquehonite is the first phase to precipitate in the Mg-CO_2-H_2O system at 25°C, in the presence or absence of cyanobacteria (Mavromatis *et al*., 2012; Hopkinson *et al*., 2012; Shirokova *et al*., 2013).

Variations of DIC, Si and Mg concentrations were calculated between the beginning and the end of the main precipitation stage (**Table 2)** allowed assessing the ratios of DIC to Mg concentrations in the solid phase which ranged between 1.25 and 3.34. These values are higher than those of hydromagnesite (0.8) and nesquehonite (1), and consistent with a mixture of different magnesian carbonate phases. The apparent Mg rates during the fastest precipitation stage in both abiotic and biotic experiments varied between 0.61 to 1.64 mmol Mg L^{-1} day^{-1}. They are of the same order of magnitude than those calculated from the data of Shirokova et al. (2013) in Si-free solutions which varied from 0.31 to 2.88 mmol Mg L^{-1} day^{-1}.

In biotic experiments where the formation of Mg carbonate was observed, the ratio of Mg decrease to organic carbon produced ($\Delta Mg/\Delta C_{org}$) during the course of experiment was calculated considering that the proportion of carbon in dry biomass is 50%. This ratio was equal to 0.24, 0.45, 0.37, 0.22 and 0.73 for the experiments SiMg, Mg3, SiMg3, DSM and SD, respectively (see **Table 1** for abbreviation of experimental conditions). These values are inferior

to the theoretical Mg/C_{org} ratio of 1 for nesquehonite as first precipitating phase during cyanobacterial photosynthesis:

$$Mg^{2+} + 2HCO_3^- + 3H_2O = MgCO_3 \bullet 3H_2O \downarrow + CH_2O + O_2 \uparrow$$

Therefore, one can assume that the efficiency of cyanobacterially-induced precipitation of hydrous Mg carbonate is partially decreased due to the presence of aqueous Si, and a part of Mg resides within amorphous Si-Mg compounds.

4.2. Mechanisms of biomineralization and the role of sepiolite as a precursor of carbonate mineral formation

A solid fibrous phase observed via TEM in the experiment containing 10 mM of Mg and 0.4 mM of Si in presence of cyanobacteria did not show any crystalline order, however these formations strongly resembled to sepiolite recently synthesized in laboratory (Baldermann *et al.*, 2018) (**Fig. S5**). The latter study was performed under abiotic conditions at different Si/Mg ratios, and reported the precipitation of sepiolite after 2 to 3 months. One of their experiments (Si/Mg = 1/28) corresponded to Si:Mg ratio in our experiment (10 mM Mg and 0.4 mM Si). In our case, no abiotic precipitation of sepiolite was observed; presumably, the relatively short duration of the experiments (two weeks) was not sufficient to allow the abiotic formation of this mineral. However, in biotic experiments, the bacterial metabolism and the associated increase of pH could have induced the precipitation of sepiolite, via increasing the saturation index of this mineral (**Fig. 2**). This is a notable result which demonstrates a strong power of bacteria to accelerate the precipitation of minerals whose abiotic formation is thermodynamically possible but delayed because of the low rate and the kinetic barriers of nucleation. Presumably, cyanobacterial cells and their exopolysaccharides can act as mineral nucleation centers by decreasing activation energies (Dupraz *et al.*, 2009) thus rendering possible the precipitation of sepiolite already after the first week of incubation.

Another interesting result of this study is that the sepiolite can serve as a precursor of hydrous Mg carbonate formation. According to the EDS analysis of the biotic experiment reaction products (**Figs. 4D, 5D**), the sepiolite (or sepiolite-like amorphous material) decreased its relative abundance between 1 and 2 weeks of incubation as reflected in a ten-fold decrease of Si concentration in the solid phase. This observation is consistent with a hypothesis of hydrous Mg silicate providing Mg for in-situ hydrous Mg carbonate precipitation via coupled dissolution/precipitation reaction. Such an explanation was recently put forward by Pace *et al*. (2016) to explain in-situ dolomite/protodolomite formation in the vicinity of natural biofilm producing both Mg, Ca carbonate, protodolomite and sepiolite.

The dark spheric formations observed inside the cells of cyanobacteria (**Fig. 7**) were similar to amorphous calcium carbonates intracellularly precipitated by several cyanobacteria, such as *Synechococcus* sp. PCC 6312 or *Synechococcus* sp. PCC 6716 (Benzerara *et al.*, 2014). However, according to a former study of the precipitation of secondary minerals in presence of *Synechococcus* sp. PCC 7942, these were phosphate globules, initially present in the cells before the beginning of the experiments (Lamérand *et al.*, 2020).

In abiotic experiments, the increase of pH via the addition of NaOH led to the precipitation of the same minerals than those formed during biotic experiments, thus indicating that the main driving factor of biomineralization is the photosynthetically-induced pH increase. However, production of alkaline microenvironment is certainly necessary but not sufficient for extracellular Mg silicate and carbonate formation. Indeed, separating the cyanobacteria from the bulk of aqueous solution via enclosing them in the dialysis bag (< 2-3 nm pore size) yielded the precipitation solely inside the dialysis compartment (**Fig. S1**), despite of identical chemical composition of aqueous solution (pH, Mg, DIC, saturation state) inside and outside the dialysis compartment. This strongly suggests that cyanobacterial cells and their EPS which were retained by dialysis membrane, serve as nucleation centers to promote the mineralization. As

such, the limiting step of bio-carbonation could be the presence of bacterial cells whose surfaces provided a template for nucleation. Another explanation could be that Mg-carbonate / Mg-silicate nucleation clusters that were formed in the microenvironment around the cells inside the dialysis bag were too large to pass through the pores of the dialysis membrane, and thus the majority of precipitation occurred in the bulk of bacterial suspension.

The processes of precipitation of magnesian carbonates by cyanobacteria could be similar to those of calcium carbonates. The latter are well studied in various phototrophic bacterial systems (Aloisi, 2008; Bundeleva *et al*., 2014; Cam *et al*., 2018; Dittrich *et al*., 2003; 2004; Lee *et al*., 2006). Following this path, we suggest that, first, Mg^{2+} ions accumulate at the surface of the cells because of electrostatic interactions between the negatively charged groups of the cells surface (carboxylates, hydroxylates, phosphorylates) and the Mg^{2+} cations (Douglas and Beveridge, 1998). This is further stimulated by the presence of EPS which could act as nucleation centers (Dittrich and Obst, 2004), via decreasing the interfacial energy and providing sizeable amount of cation-binding moieties (Priester *et al*., 2006; Guibaud *et al*., 2008; Kantar *et al*., 2011). Aqueous carbonate and bicarbonate anions may interact with these cations to form carbonate minerals, near the cells and in their capsules (Miller *et al.*, 1990). Another possible mechanism, suggested for the first time by Douglas and Beveridge (1998) for *Synechococcus* cells suspended in Fayetteville Green Lake water and producing massive gypsum or calcite deposits is the continuous release of mineralized S-layer by the cells, quickly replaced by new polymeric molecules. This may produce biominerals located at some distances from the cell surfaces, as also seen in our TEM images. Such a pathway does not require any specific protection mechanism against cell encrustation by newly formed minerals, unlike the one which operates for $CaCO_3$ - *Synechococcus* sp. system (Martinez *et al*., 2010; Bundeleva et al., 2014). Presumably, hydrous Mg carbonates formed in the vicinity of photosynthesizing cells,

essentially over external EPS templates, are not capable of creating full cell encrustation and entombment.

To resume, macroscopic experiments, thermodynamic calculations and TEM observations suggest the following mechanism. First, an amorphous magnesium silicate and nanocrystals of Mg carbonates are formed around the cells, then these precursors are dissolved, liberating Mg in the fluid. Nanocrystals of nesquehonite are formed in the vicinity of the cells, and they gradually assemble themselves into thin needles. Over time, a part of these crystals could transform into more stable magnesium carbonate such as hydromagnesite.

4.3. CO_2 sequestration capacity via hydrous Mg carbonate biomineralization by cyanobacteria

During the CO_2 biomineralization by cyanobacteria, carbon can be sequestered (i.e., removed from solution) via two pathways: as organic carbon (C_{org}) during the production of biomass (both the biomass and soluble exometabolites), and as inorganic carbon (C_{inorg}) during the formation of carbonate minerals. The quantity of sequestered C_{inorg} was estimated via mass-balance calculation from a decrease of DIC concentration between the beginning and the end of the experiment. The amount of C_{org} formed in the experiment is composed of particulate organic carbon (POC) which corresponds to half of the dry biomass, and DOC in the form of exometabolites and EPS. Carbon sequestration potential (CSP) was calculated via dividing the quantity of sequestered carbon by the time it took to be sequestered. We estimated that carbon was mostly (ca 60-70%) sequestered in particulate organic form (**Fig. 9**). Soluble exometabolites and EPS (DOC) contributed to only 2-10% of the total CSP. The quantity of C sequestered in the mineral form (as DIC) was similar in biotic and abiotic experiments (0.7-1.2 mmol L^{-1} day^{-1}). The presence of Si in the solution slightly increased (~20%) the quantity of sequestered inorganic carbon, whereas there was no correlation between the quantity of aqueous

Mg in the initial solution and the CSP. Overall, biotic experiments with nutritive medium and without dialysis bags (Mg3, SiMg3 and SiMg) exhibited the highest carbon sequestration potential because of the large quantity of C sequestered in the biomass during the development of cyanobacteria. This shows the potential of cyanobacteria to sequester carbon, by both the biomass they produce and the carbonate minerals they stimulate to precipitate whereas in abiotic environment, an external addition of NaOH was necessary to form carbonate minerals.

5. Conclusions

The biomineralization of carbon dioxide is an important process to consider in CO_2 storage and sequestration techniques. During this study, the role of cyanobacteria in the precipitation of carbonate phases was examined at variable biological and physicochemical parameters (cyanobacterial biomass, pH, Mg, Si, DIC, DOC) over 10 to 14 days of reaction. The rates of Mg carbonate precipitation were comparable to those observed in previous experiments with Si-free aquatic systems of Mg carbonates and cyanobacteria and were unaffected by Mg:Si ratio in the initial solution.

Obtained results demonstrate strong control of the cyanobacterial activity on hydrous carbonate (nesquehonite and hydromagnesite) and Mg silicate mineral precipitation. The dominant mechanisms include the increase in pH near the cells during the photosynthesis and the release of exopolymers that can serve as nucleation centers and thus trigger carbonates and silicates precipitation from supersaturation solution. The dialysis experiments demonstrated incontestable role of cyanobacterial surfaces, serving as templates for both Mg silicate and carbonate precipitation. The TEM observations highlighted the formation of crystalline magnesian carbonated phases in the vicinity of cells. The minerals formed could be a mixture of nesquehonite and hydromagnesite. A magnesium silicate such as sepiolite or its poorly crystalline analogue could also be present at the beginning of biomineralization reaction. This

suggests its possible role as a precursor of carbonate minerals, which is consistent with recent natural observations. The overall C sequestration in the organic and mineral form was dominated by particulate organic C (in the form of bacterial biomass) with ca. 35% of C sequestered in the form of hydrous Mg carbonates.

Acknowledgements :

Supports from grants BIOCASTRO of MITI (CNRS), SERPCARB (Carnot ISIFoR), BIOMIN (Interrvie INSU-CNRS) and CaBioCa of Défi (Action conjointe, MITI CNRS) are acknowledged.

References

Aloisi, G., 2008. The calcium carbonate saturation state in cyanobacterial mats throughout Earth's history. Geochim. Cosmochim. Acta 72, 6037–6060.

Balan, E., Noireaux, J., Mavromatis, V., Saldi, G., Montouillout, V., Blanchard, M., Pietrucci, F., Gervais, C., Rustad, J.R., Schott, J., Gaillardet, J., 2018. Theoretical isotopic fractionation between structural boron in carbonates and aqueous boric acid and borate ion. Geochim. Cosmochim. Acta 222, 117-129.

Baldermann, A., Mavromatis, V., Frick, P.M., Dietzel, M., 2018. Effect of aqueous Si/Mg ratio and pH on the nucleation and growth of sepiolite at 25°C. Geochim. Cosmochim. Acta 227, 211–226.

Balogh-Brunstad, Z., Keller, K.C., Dickinson, J.T., Stevens, F., Li, C.Y., Bormann, B.T., 2008. Biotite weathering and nutrient uptake by ectomycorrhizal fungus, *Suillus tomentosus*, in liquid-culture experiments. Geochim. Cosmochim. Acta 72, 2601–2618.

Barbiero, L., Queiroz Neto, J.P., Ciornei, G., Sakamoto, A.Y., Capellari, B., Fernandes, E., Valles, V., 2002. Geochemistry of water and ground water in the Nhecolândia, Pantanal of Mato Grosso, Brazil: variability and associated processes. Wetlands 22, 528-540.

Barbiero, L., Rezende Filho, A., Furquim, S.A.C., Furian, S., Sakamoto, A.Y., Valles, V., Graham, R.C., Fort, M., Ferreira, R.P.D., Queiroz Neto, J.P., 2008. Soil morphological control on saline and freshwater lake hydrogeochemistry in the Pantanal of Nhecolândia, Brazil. Geoderma 148, 91-106.

Bénézeth, P., Saldi, G., Dandurand, J.L., Schott, J., 2011. Experimental determination of the solubility product of magnesite at 50 to 200°C. Chem. Geol. 286, 21-31.

Bénézeth, P., Godard, M., Thinon, I.P., Gouze, P., Wolff-Boenisch, D., Laurent, L., Cluzel, D., Audigane ,P., Monnin, C., Augé, T., Ménez, B., Baby, P., Kelemen, P., 2014. Report of the project "Stockage Géologique du CO_2 in situ en Nouvelle-Calédonie ». CNRT Nickel et Environnement. 83 pp.

Bénézeth, P., Stefánsson, A., Gautier, Q., Schott, J., 2013. Mineral solubility and aqueous speciation under hydrothermal conditions to 300°C – The carbonate system as an example. Rev. Min. Geochem. 76, 81-133.

Bénézeth, P., Berninger, N., Bovet, N., Schott, J., Oelkers, E.H., 2018. Experimental determination of the solubility product of dolomite at 50 to 250°C. Geochim. Cosmochim. Acta 224, 262-275.

Benzerara, K., Skouri-Panet, F., Li, J., Férard, C., Gugger, M., Laurent, T., Couradeau, E., Ragon, M., Cosmidis, J., Menguy, N., Margaret-Oliver, I., Tavera, R., López-Garcia, P., Moreira, D., 2014. Intracellular Ca-carbonate biomineralization is widespread in cyanobacteria. P. Natl. Acad. Sci. USA 111, 10933–10938.

Blum, A., Lasaga, A., 1988. Role of surface speciation in the low-temperature dissolution of minerals. Nature 331, 431–433.

Bundeleva, I.A., Shirokova, L.S., Pokrovsky, O.S., Bénézeth, P., Ménez, B., Gérard, E., Balor, S., 2014. Experimental modeling of calcium carbonate precipitation by cyanobacterium *Gloeocapsa* sp.. Chem. Geol. 374–375, 44–60.

Cam, N., Benzerara, K., Georgelin, T., Jaber, M., Lambert, J.F., Poinsot, M., Skouri-Panet, F., Moreira, D., López-García, P., Raimbault, E., Cordier, L., Jézéquel, D., 2018. Cyanobacterial formation of intracellular Ca-carbonates in undersaturated solutions. Geobiology 16, 49–61.

Dhami, N.K., Reddy, M.S., Mukherjee, A., 2014. Synergetic role of bacterial urease and carbonic anhydrase in carbonate mineralization. Appl. Biochem. Biotechnol. 172(5), 2552-2561.

Dittrich, M., Kurz, P., Wehrli, B., 2004. The role of autotrophic picocyanobacteria in calcite precipitation in an oligotrophic lake. Geomicrobiol. J. 21, 45–53.

Dittrich, M., Müller, B., Mavrocordatos, D., Wehrli, B., 2003. Induced calcite precipitation by cyanobacterium *Synechococcus*. Acta Hydroch. Hydrob. 31, 162–169.

Dittrich, M., Obst, M., 2004. Are picoplankton responsible for calcite precipitation in lakes? Ambio 33, 559–564.

Douglas, S., Beveridge, T.J., 1998. Mineral formation by bacteria in natural microbial communities. FEMS Microbiol. Ecol. 26, 79–88.

Dupraz, C., Reid, R.P., Braissant, O., Decho, A.W., Norman, R.S., Visscher, P.T., 2009. Processes of carbonate precipitation in modern microbial mats. Earth Sci. Rev. 96(3), 141–162.

Ganor, J., Reznik, I.J., Rosenberg, Y.O., 2009. Organics in water-rock interactions. Rev. Mineral. Geochem. 70, 259–369.

Gautier, Q., Bénézeth, P., Mavromatis, V., Schott, J., 2014. Hydromagnesite solubility product and growth kinetics in aqueous solution from 25 to 75°C. Geochim. Cosmochim. Acta 138, 1-20.

Guibaud, G., Bordas, F., Saaid, A., D'abzac, P., Van Hullebusch, E., 2008. Effect of pH on cadmium and lead binding by extracellular polymeric substances (EPS) extracted from environmental bacterial strains. Colloid Surface B 63, 48-54.

Han, Z., Yan, H., Zhou, S., Zhao, H., Zhang, Y., Zhang, N., Yao, C., Zhao, L., Han, C., 2013. Precipitation of calcite induced by *Synechocystis* sp. PCC6803. World J. Microb. Biot. 29, 1801–1811.

Harrison, A.L., Mavromatis, V., Oelkers, E.H., Bénézeth, P., 2019. Solubility of the hydrated Mg-carbonates nesquehonite and dypingite from 5 to 35°C: Implications for CO_2 storage and the relative stability of Mg-carbonates. Chem Geol 504, 123-135.

He, W., Zhang, L., Liu, H., Zhang, Y., Fu, B., Zhang, X., Juang, Q., 2022. CO_2 sequestration mediated by wollastonite in anaerobic digestion of sewage sludge: From sequence batch to semi-continuous operation. Chemosphere 287(3), Art No 132095. https://doi.org/10.1016/j.chemosphere.2021.132095.

Hopf, J., Langenhorst, F., Pollok, K., Merten, D., Kothe, E., 2009. Influence of microorganisms on biotite dissolution: an experimental approach. Chem. der Erde – Geochem., 69, 45–56.

Hopkinson, L., Kristovab, P., Ruttb, K., Cressey, G., 2012. Phase transitions in the system $MgO–CO_2–H_2O$ during CO_2 degassing of Mg-bearing solutions. Geochim. Cosmochim. Acta 76, 1–13.

Hutchens, E., 2009. Microbial selectivity on mineral surfaces: possible implications for weathering processes. Fungal Biol. Rev. 23, 115–121.

Jansson, C., Northen, T., 2010. Calcifying cyanobacteria—the potential of biomineralization for carbon capture and storage. Curr. Opin. Biotech. 21, 365–371.

Kantar, C., Demiray, H., Dogan, N.M., Dodge, C.J., 2011. Role of microbial exopolymeric substances (EPS) on chromium sorption and transport in heterogeneous subsurface soils: I. Cr(III) complexation with EPS in aqueous solution. Chemosphere 82, 1489–1495.

Kelemen, P.B., Matter, J., Streit, E.E., Rudge, J.F., Curry, W.B., Blusztajn, J., 2011. Rates and mechanisms of mineral carbonation in peridotite: natural processes and recipes for enhanced, in situ CO_2 capture and storage. Annu. Rev. Earth Pl. Sc. 39, 545-576.

Lamérand, C., Shirokova, L.S., Bénézeth, P., Rols, J.L., Pokrovsky, O.S., 2020. Olivine dissolution and hydrous Mg carbonate and silicate precipitation in the presence of microbial consortium of photo-autotrophic and heterotrophic bacteria. Geochim. Cosmochim. Acta 268, 123–141.

Lee, B.D., Apel, W.A., Walton, M.R., 2004. Screening of cyanobacterial species for calcification. Biotechnol. Prog. 20, 1345–1351

Lee, B.D., Apel, W.A., Walton, M.R., 2006. Calcium carbonate formation by *Synechococcus* sp. strain PCC 8806 and *Synechococcus* sp. strain PCC 8807. Bioresource Technol. 97, 2427–2434.

Luce, R.W., Bartlett, R.W., Parks, G.A., 1972. Dissolution kinetics of magnesium silicates. Geochim. Cosmochim. Acta 36, 35–50.

Ludwig, R, Al-Horani, F., de Beer, D., Jonkers, H.M., 2005. Photosynthesis-controlled calcification in hypersaline microbial mat. Limnol. Oceanogr. 50, 1836–1843.

Martinez, R.E., Gardés, E., Pokrovsky, O.S., Schott, J., Oelkers, E.H., 2010. Do photosynthetic bacteria have a protective mechanism against carbonate precipitation at their surfaces? Geochim. Cosmochim. Acta 74, 1329–1337.

Martinez, R.E., Weber, S., Grimm, C., 2016. Effects of freshwater *Synechococcus* sp. cyanobacteria pH buffering on $CaCO_3$ precipitation: implications for CO_2 sequestration. Appl. Geochem. 75, 76-89.

Matter, J.M., Kelemen, P.B., 2009. Permanent storage of carbon dioxide in geological reservoirs by mineral carbonation. Nat. Geosci. 2, 837–841.

Matter, J.M., Broecker, W.S., Stute, M., Gislason, S.R., Oelkers, E.H., Stefansson, A., Wolff-Boenisch, D., Gunnlaugsson, E., Björnsson, G.A., 2009. Permanent carbon dioxide storage into basalt: The CarbFix Pilot Project, Iceland. Energy Procedia, 1(1), 3641-3646.

Mavromatis, V., Pearce, C.R., Shirokova, L.S., Bundeleva, I.A., Pokrovsky, O.S., Bénézeth, P., Oelkers, E.H., 2012. Magnesium isotope fractionation during hydrous magnesium carbonate precipitation with and without cyanobacteria. Geochim. Cosmochim. Acta 76, 161-174.

McCutcheon, J., Power, I.M., Harrison, A.L., Dipple, G.M., Southam, G., 2014. A greenhouse-scale photosynthetic microbial bioreactor for carbon sequestration in magnesium carbonate minerals. Environ. Sci. Technol. 48, 9142–9151.

Mittchel, A.C., Dideriksen, K., Spangler, L.H., Cunningham, A.B., Gerlach, R., 2010. Microbially enhanced carbon capture and storage by mineral-trapping and solubility-trapping. Environ. Sci. Technol. 44(13), 5270-5276.

Miller, A.G., Espie, G.S., Canvin, D.T., 1990. Physiological aspects of CO_2 and HCO_3^- transport by cyanobacteria: a review. Can. J. Botany 68, 1291–1302.

Millero, F., Huang, F., Graham, T., Pierrot, D., 2007. The dissociation of carbonic acid in NaCl solutions as a function of concentration and temperature. Geochim. Cosmochim. Acta 71, 46‑55.

Naveed, M., Duan, J., Uddin, S., Suleman, M., Hui, Y., Li, H., 2020. Application of microbially induced calcium carbonate precipitation with urea hydrolysis to improve the mechanical properties of soil. Ecol. Eng. 153, Art No 105885. https://doi.org/10.1016/j.ecoleng.2020.105885.

Nutman, A.P., Bennett, V.C., Friend, C.R.L., Van Kranendonk, M.J., Chivas, A.R., 2016. Rapid emergence of life shown by discovery of 3,700-million-year-old microbial structures. Nature 537, 535–538.

Oelkers, E.H., 2001. An experimental study of forsterite dissolution kinetics as a function of temperature and aqueous Mg and Si concentration. Chem. Geol. 175, 485–494.

Oelkers, E.H., Gislason, S.R., Matter, J., 2008. Mineral carbonation of CO_2. Elements 4, 333–337.

Pace, A., Bourillot, R., Bouton, A., Vennin, E., Braissant, O., Dupraz, C., Duteil, T., Bundeleva, I., Patrier, P., Galaup, S., Yokoyama, Y., Franceschi, M., Virgone, A., Visscher, P.T., 2018. Formation of stromatolite lamina at the interface of oxygenic-anoxygenic photosynthesis. Geobiology 16, 378–398.

Pace, A., Bourillot, R., Bouton, A., Vennin, E., Galaup, S., Bundeleva, I., Patrier, P., Dupraz, C., Thomazo, C., Sansjofre, P., Yokoyama, Y., Franceschi, M., Anguy, Y., Pigot, L., Virgone, A., Visscher, P.T., 2016. Microbial and diagenetic steps leading to the mineralisation of Great Salt Lake microbialites. Sci. Rep. 6, 31495.

Palmer, D.A., Wesolowski, D.J., 1997. Potentiometric measurements of the first hydrolysis quotient of magnesium (II) to 250°C and 5 molal ionic strength (NaCl). J. Solution Chem. 26, 217‑232.

Pan, S.Y., Chiang, P.C., Pan, W., Kim, H., 2018. Advances in state-of-art valorization technologies for captured CO_2 towards sustainable carbon cycle. Critical Rev. Environ. Sci. Technol. 48(5), 471-534.

Parkhurst, D.L., Appelo, C.A.J., 1999. User's guide to PHREEQC (Version 2)—A computer program for speciation, batch-reaction, one-dimensional transport, and inverse geochemical calculations. U.S. Geological Survey Water-Resources Investigations Report 99-4259, 312 pp.

Peuble, S., Andreani, M., Godard, M., Gouze, P., Barou, F., Van de Moortele, B., Mainprice, D., Reynard, B., 2015. Carbonate mineralization in percolated olivine aggregates: linking effects of crystallographic orientation and fluid flow. Amer. Mineral. 100, 474-482.

Pires, J.C.M., Alvin-Ferraz, M.C.M., Martins, F.G., Simoes, M., 2012. Carbon dioxide capture from flue gases using microalgae: Engineering aspects and biorefinery concept. Renew. Sust. Energy Rev. 16(5), 3043-3053.

Plee, K, Pacton, M, Ariztegui D., 2010. Discriminating the role of photosynthetic and hetero-trophic microbes triggering low-Mg calcite precipitation in freshwater biofilms (Lake Geneva, Switzerland). Geomicrobiol. J. 27, 391–399.

Pokrovsky, O.S., Savenko, V.S., 1995. Experimental modeling of $CaCO_3$ precipitation at the conditions of photosynthesis in seawater. Oceanology 35, N6, 805-810.

Pokrovsky, O.S., Schott, J., 2000a. Forsterite surface composition in aqueous solutions: a combined potentiometric, electrokinetic, and spectroscopic approach. Geochim. Cosmochim. Acta 64, 3299–3312.

Pokrovsky, O.S., Schott, J., 2000b. Kinetics and mechanism of forsterite dissolution at 25°C and pH from 1 to 12. Geochim. Cosmochim. Acta 64, 3313–3325.

Power, I.M., Wilson, S.A., Thom, J.M., Dipple, G.M., Gabites, J.E., Southam, G., 2009. The hydromagnesite playas of Atlin, British Columbia, Canada: a biogeochemical model for CO_2 sequestration. Chem. Geol. 260, 286–300.

Power, I.M., Wilson, S.A., Small, D.P., Dipple, G.M., Wan, W., Southam, G., 2011. Microbially mediated mineral carbonation: roles of phototrophy and heterotrophy. Environ. Sci. Technol. 45, 20, 9061-9068.

Priester, J.H., Olson, S.G., Webb, S.M., Neu, M.P., Hersman, L.E., Holden, P.A., 2006. Enhanced exopolymer production and chromium stabilization in *Pseudomonas putida* unsaturated biofilms. Appl. Environ. Microbiol. 72, 1988-1996.

Revsbech, N.P., Jorgensen, B.B., Blackburn, T.H., Cohen, Y., 1983. Microelectrode studies of the photosynthesis and O_2, H_2S, and pH profiles of a microbial mat. Limnol. Oceanogr. 28, 1062–1074.

Robert, M., Berthelin, J., 1986. Role of biological and biochemical factors in soil mineral weathering. SSSA spec. publ. 17, 453–495.

Saneiyan, S., Ntarlagianni, D., Ohan, J., Lee, J., Colwell, F., Burns, S., 2019. Induced polarization as a monitoring tool for in-situ microbial induced carbonate precipitation (MICP) processes. Ecol. Eng. 127, 36-47.

Schott, J., Berner, R.A., 1983. X-ray photoelectron studies of the mechanism of iron silicate dissolution during weathering. Geochim. Cosmochim. Acta 47, 2233–2240.

Shirokova, L.S., Bénézeth, P., Pokrovsky, O.S., Gerard, E., Ménez, B., Alfredsson, H., 2012. Effect of the heterotrophic bacterium *Pseudomonas reactans* on olivine dissolution kinetics and implications for CO_2 storage in basalts. Geochim. Cosmochim. Acta 80, 30–50.

Shirokova, L.S., Mavromatis, V., Bundelava, I.A., Pokrovsky, O.S., Bénézeth, P., Gérard, E., Pearce, C.R., Oelkers, E.H., 2013. Using Mg isotopes to trace cyanobacterially mediated magnesium carbonate precipitation in alkaline lakes. Aquat. Geochem. 19, 1-24.

Shirokova, L.S., Labouret, J., Gurge, M., Gérard, E., Ivanova, I.S., Zabelina, S.A., Pokrovsky, O.S., 2017. Impact of cyanobacterial associate and heterotrophic bacteria on dissolved organic carbon and metal in moss and peat leachate: Application to permafrost thaw in aquatic environments. Aquat. Geochem. 23, 331–358.

Sissmann, O., Daval, D., Brunet, F., Guyot, F., Verlaguet, A., Pinquier, Y., Findling, N., Martinez, I., 2013. The deleterious effect of secondary phases on olivine carbonation yield: Insight from time-resolved aqueous-fluid sampling and FIB-TEM characterization. Chem. Geol. 357, 186-202.

Stanier, R.Y., Deruelles, J., Rippka, R., Herdman, M., Waterbury, J.B., 1979. Generic assignments, strain histories and properties of pure cultures of cyanobacteria. Microbiology 111, 1–61.

Stefánsson, A., Bénézeth, P., Schott, J., 2013. Carbonic acid ionization and the stability of sodium bicarbonate and carbonate ion pairs to 200°C– A potentiometric and spectrophotometric study. Geochim. Cosmochim. Acta 120, 600-611.

Stefánsson, A., Bénézeth, P., Schott, J., 2014. Potentiometric and spectrophotometric study of the stability of magnesium carbonate and bicarbonate ion pairs to 150°C and aqueous inorganic carbon speciation and magnesite solubility. Geochim. Cosmochim. Acta 138, 21-31.

Stockmann, G.J., Shirokova, L.S., Pokrovsky, O.S., Oelkers, E.H., Bénézeth, P., Bovet, N., Gislason, S., 2011. Does the presence of heterotrophic bacterium *Pseudomonas reactans* affect basaltic glass dissolution rates? Chem. Geol. 296-297, 1-18.

Sun, X., Alcalde, J., Gomez-Rivas, E., Struth, L., Johnson, G., Travé, A., 2020. Appraisal of CO_2 storage potential in compressional hydrocarbon-bearing basins: Global assessment and case study in the Sichuan Basin (China). Geoscience Front. 11, 2309-2321.

771 Sverdrup, H., 2009. Chemical weathering of soil minerals and the role of biological processes.
772 Fungal Biol. Rev. 23, 94–100.
773 Thompson, J.B., Ferris, F.G., 1990. Cyanobacterial precipitation of gypsum, calcite, and
774 magnesite from natural alkaline lake water. Geology 18, 995–998.
775 Thorseth, I.H., Furnes, H., Heldal, M., 1992. The importance of microbiological activity in the
776 alteration of natural basaltic glass. Geochim. Cosmochim. Acta 56, 845–850.
777 Uroz, S., Calvaruso, C., Turpault, M.P., Frey-Klett, P., 2009. Mineral weathering by bacteria:
778 ecology, actors and mechanisms. Trends Microbiol. 17, 378–387.
779 Valsami-Jones, E., McEldowney, S., Cotter-Howells, J., Campbell, L., Batchelder, M., 2000.
780 Mineral dissolution by heterotrophic bacteria: principles and methodologies. Min. Soc. Ser.
781 2000, 27-55.
782 Zhu, T., Paulo, C., Merroun, M.L., Dittrich, M., 2015. Potential application of biomineralization
783 by Synechococcus PCC8806 for concrete restoration. Ecol. Eng. 82, 459-468.
784 Zhu, T., Lin, Y., Lu, X., Dittrich, M., 2018. Assessment of cyanobacterial species for carbonate
785 precipitation on mortar surface under different conditions. Ecol. Eng. 120, 154–163.
786 https://doi.org/10.1016/j.ecoleng.2015.05.017.
787 Zhuang, D., Yan, H., Tucker, M.E., Zhao, H., Han, Z., Zhao, Y., Sun, B., Li, D., Pan, J., Zhao,
788 Y., Meng, R., Shan, G., Zhang, X., Tang, R., 2018. Calcite precipitation induced by
789 *Bacillus cereus* MRR2 cultured at different Ca^{2+} concentrations: Further insights into biotic
790 and abiotic calcite. Chem. Geol. 500, 64-87.
791
792

Table 1. List of conducted experiments, chemical composition of experimental solutions, bacteria status and reactor type. All the experiments were run in the diluted BG-11 (10%) nutrient medium.

Nom	$NaHCO_3$, mM	Mg, mM	Si, mM	Cyanobacteria	Experimental conditions
SiMg	10	5	0.3	1 g_{wet}/L *Synechococcus* sp.	Aerated, mixed
Mg3	10	10	-	1 g_{wet}/L *Synechococcus* sp.	Aerated, mixed
SiMg3	10	10	0.4	1 g_{wet}/L *Synechococcus* sp.	Aerated, mixed
ASiMg	10	5	0.3	Bacteria-free	Aerated, mixed
AMg3	10	10	-	Bacteria-free	Aerated, mixed
ASiMg3	10	10	0.4	Bacteria-free	Aerated, mixed
BSM	10	10	-	1 g_{wet}/L *Synechococcus* sp.	Aerated, mixed
CSM	10	10	-	1 g_{wet}/L *Synechococcus* sp.	Aerated, mixed, reactors kept in darkness
DSM	10	10	-	1 g_{wet}/L *Synechococcus* sp.	Bacteria inside the dialysis bag
SD	10	10	-	1 g_{wet}/L *Synechococcus* sp.	Bacteria outside the dialysis bag

Table 2. Variations of concentrations of DIC, Mg and Si and rates of Mg, Si and DIC concentrations decrease (respectively R_{Mg}, R_{Si} and R_{DIC}, mmol L^{-1} day^{-1}) during the stage of maximal concentration change (mineral precipitation).

	ΔDIC, mM	Δ[Mg], mM	Δ[Si], mM	ΔDIC/Δ[Mg]	Δ[Mg]/Δ[Si]	R_{Mg}	R_{Si}	R_{DIC}
SiMg	8.32	4.51	0.29	1.85	15.6	0.76	-0.10	1.41
Mg3	7.50	4.91	-	1.53	-	1.51	-	2.33
SiMg3	9.88	5.49	0.26	1.80	21.1	1.19	-0.12	1.66
ASiMg	5.82	2.54	0.44	2.29	5.77	0.62	-0.21	1.40
AMg3	4.83	1.81	-	2.67	-	0.69	-	2.09
ASiMg3	5.67	1.70	0.58	3.34	2.93	0.96	-0.27	1.40
BSM	-	-	-	-	-	-	-	-
CSM	8.64	6.31	-	1.37	-	1.64	-	1.43
DSM	-	-	-	-	-	-	-	-
SD	5.13	4.11	-	1.25	-	0.61	-	1.28

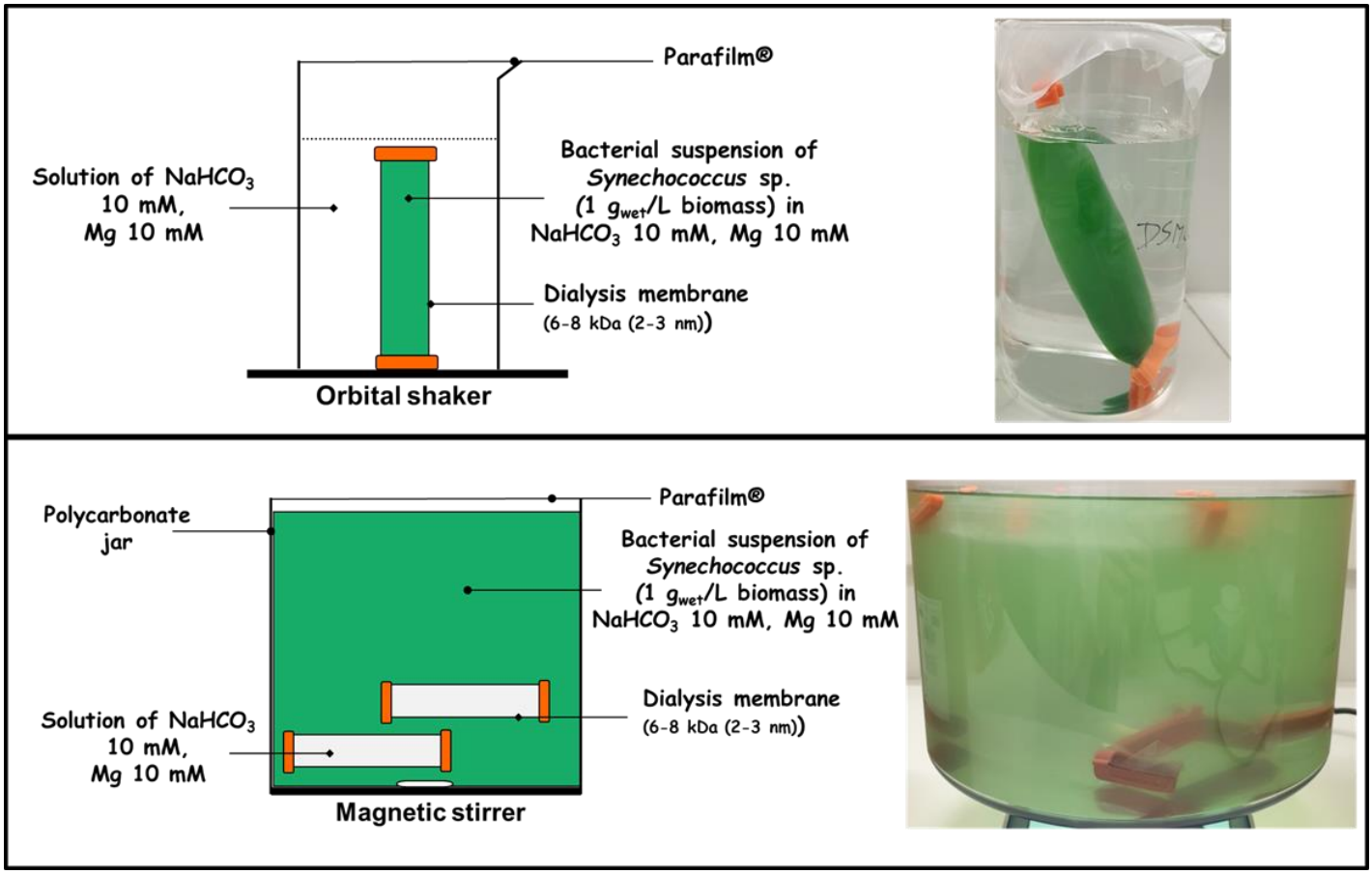

Figure 1. Schematic representations and photos of experiments with cyanobacteria *Synechococcus* sp. inside (A, experiment DSM) or outside (B, experiment SD) of the dialysis bag.

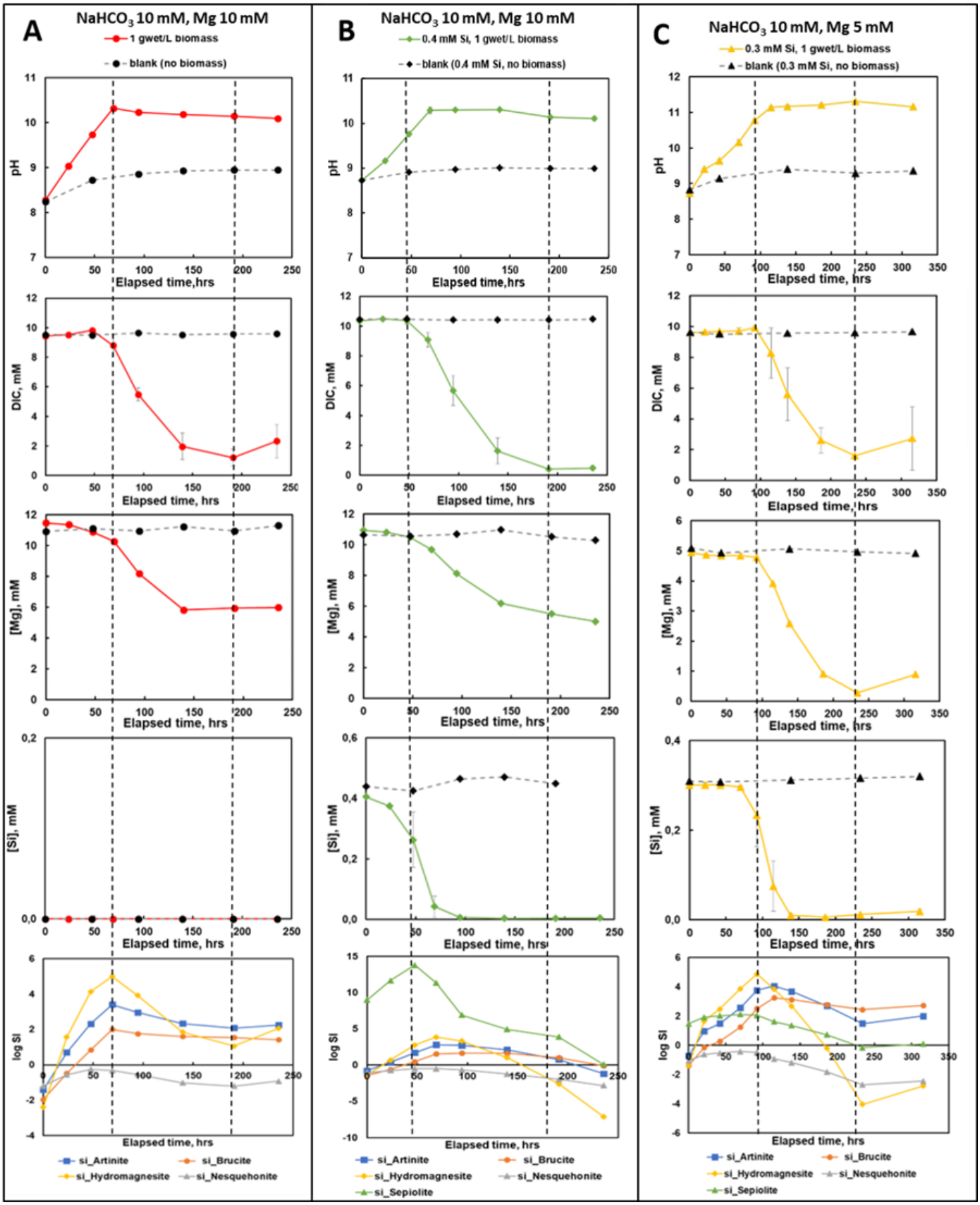

Figure 2. Evolution of pH, concentrations in DIC, Mg and Si, and saturation indices (SI) of some carbonate or silicate magnesian minerals as a function of time in experiments realized in presence of a monoculture of cyanobacteria *Synechococcus* sp. and 10% BG-11 culture medium in a solution of $NaHCO_3$ 10 mM with **A**: 10 mM Mg, **B**: 10 mM Mg and 0.4 mM Si, **C**: 5 mM Mg and 0.3 mM Si. Error bars represent standard deviation of experimental replicates.

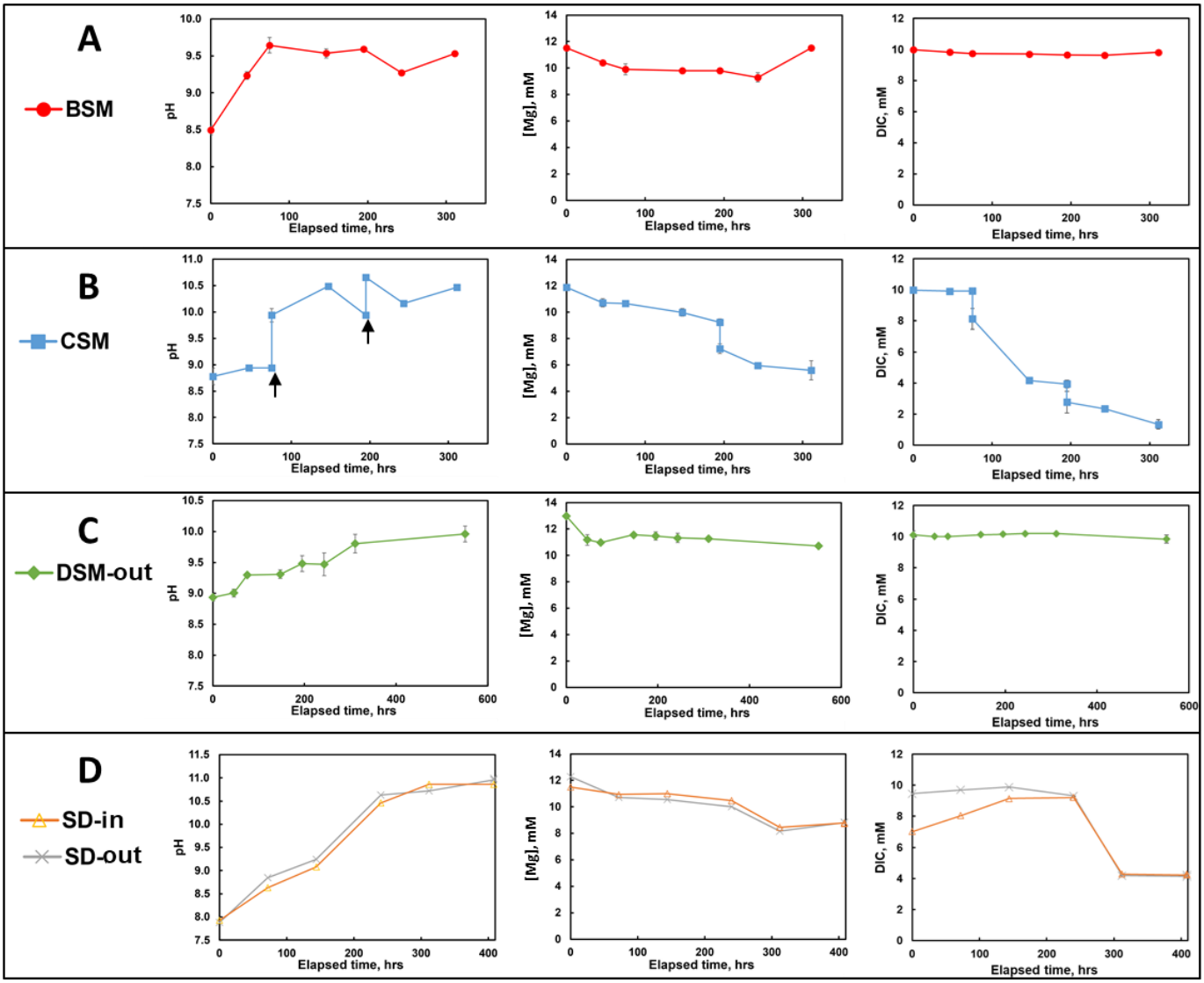

Figure 3. Evolution of pH, Mg and DIC concentrations over time for experiments without BG-11 culture media (BSM, **A**), in darkness (CSM, **B**), with cyanobacteria inside dialysis bag (DSM-out: sampling outside of the bag, **C**) and cyanobacteria outside of dialysis bag (SD-in and out: sampling respectively inside and outside of the bag, **D**). Error bars represent standard deviation of replicates.

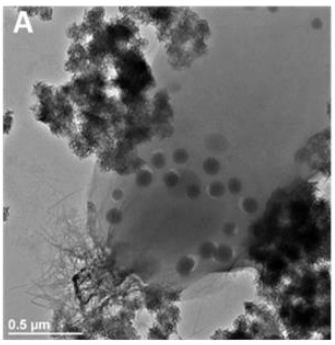

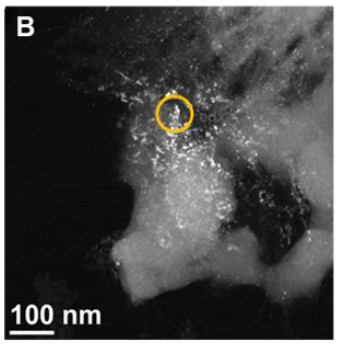

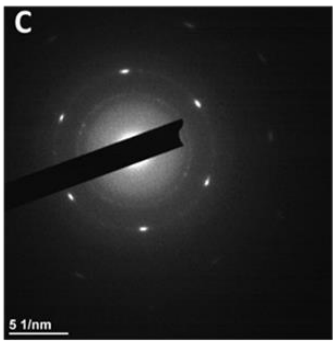

D

Element	%
Mg	41.7
Si	12.7
O	37.3
C	7.5
Cl	0.9

Figure 4. TEM observations of the experimental cell suspension with formed minerals in the presence of 10 mM of $NaHCO_3$ with 10 mM of Mg and 0.4 mM of Si after one week of experiment. **A**: cell of *Synechococcus* sp. in the center, presence of a solid fibrous phase near the cell (at the top and bottom right of the picture), and needles in the vicinity of the bacteria, **B**: picture in dark field to highlight the nanocrystals (white dots on the picture), **C**: FFT realized in the orange circle in panel B, **D**: composition of the particles in the orange circle according to the EDS analysis.

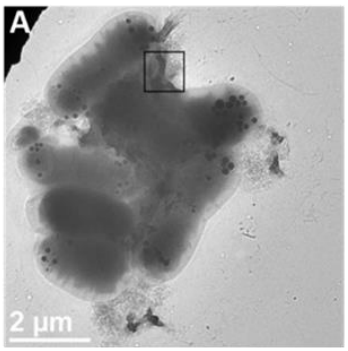

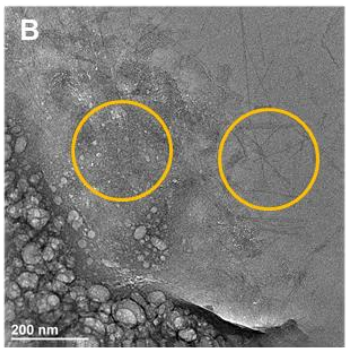

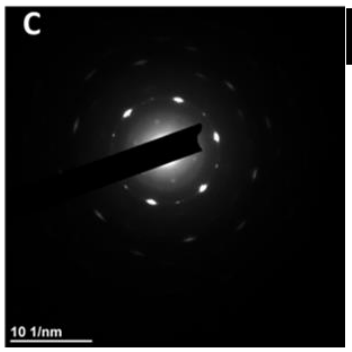

D

Element	%
Mg	46.7
Si	0.8
O	34.1
C	17.2
Cl	1.2

Figure 5. TEM observations of the experimental cell suspension with formed minerals in the presence of 10 mM of $NaHCO_3$ with 10 mM of Mg and 0.4 mM of Si after two weeks of experiments. **A**: group of cyanobacteria *Synechococcus* sp., **B**: zoom on the part framed in black on A, **C** : FFT realized on the part encircled in orange on the left on panel B, **D**: composition of the particles in the left orange circle according to the EDS analysis.

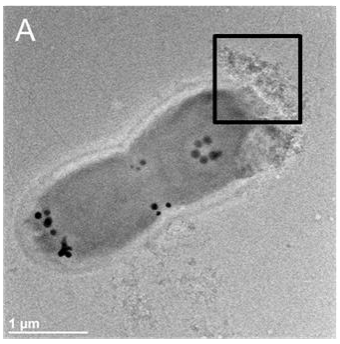

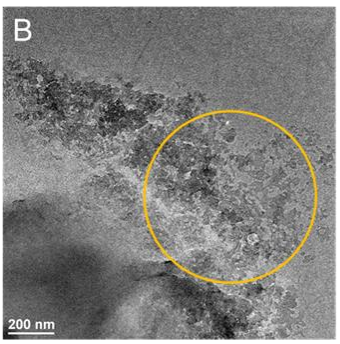

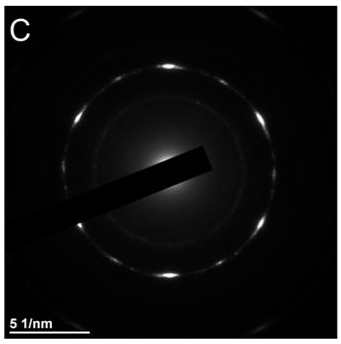

D

Element	%
Mg	37.9
O	13.2
C	47.1
Cl	1.8

Figure 6. TEM observations of bacterial cells collected outside the dialysis bags in the experiment SD. **A**: cyanobacteria *Synechococcus* sp., **B**: zoom on the part framed in black on A, **C**: FFT realized on the part circled in orange on B, **D**: composition of the particles in the orange circle according to the EDS analysis.

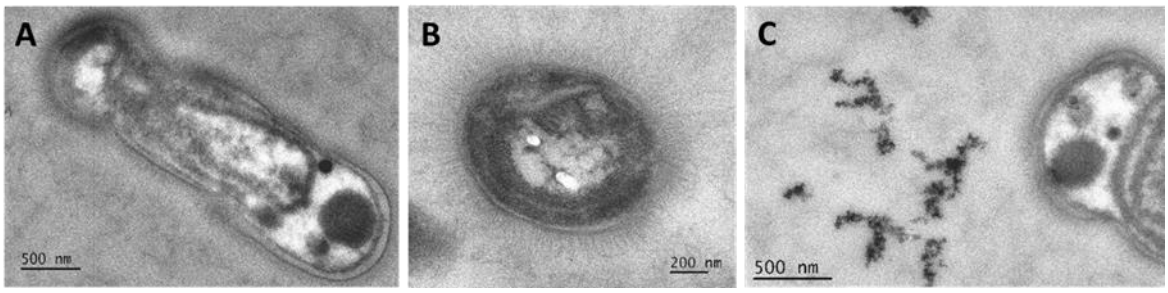

Figure 7. TEM cross-sections of *Synechococcus* sp. in a solution of 10 mM of $NaHCO_3$ enriched with 10 mM of Mg and 0.4 mM of Si. **A**: longitudinal section of *Synechococcus* sp., **B**: cross section of *Synechococcus* sp., **C**: solid particles on the left, cell of *Synechococcus* sp. on the right.

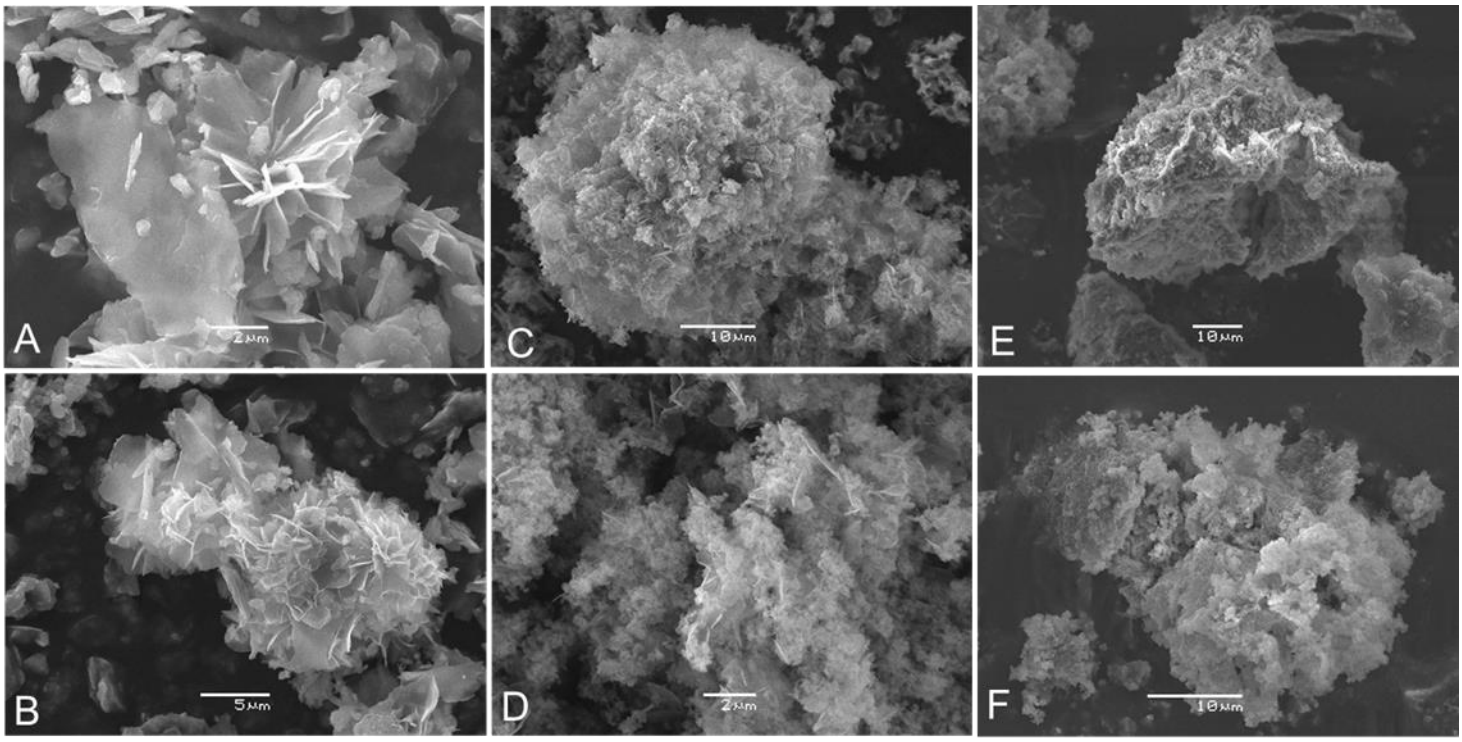

Figure 8. SEM pictures of the precipitated phases from abiotic experiments AMg3 (**A** and **B**), ASiMg3 (**C** and **D**), and ASiMg (**E** and **F**).

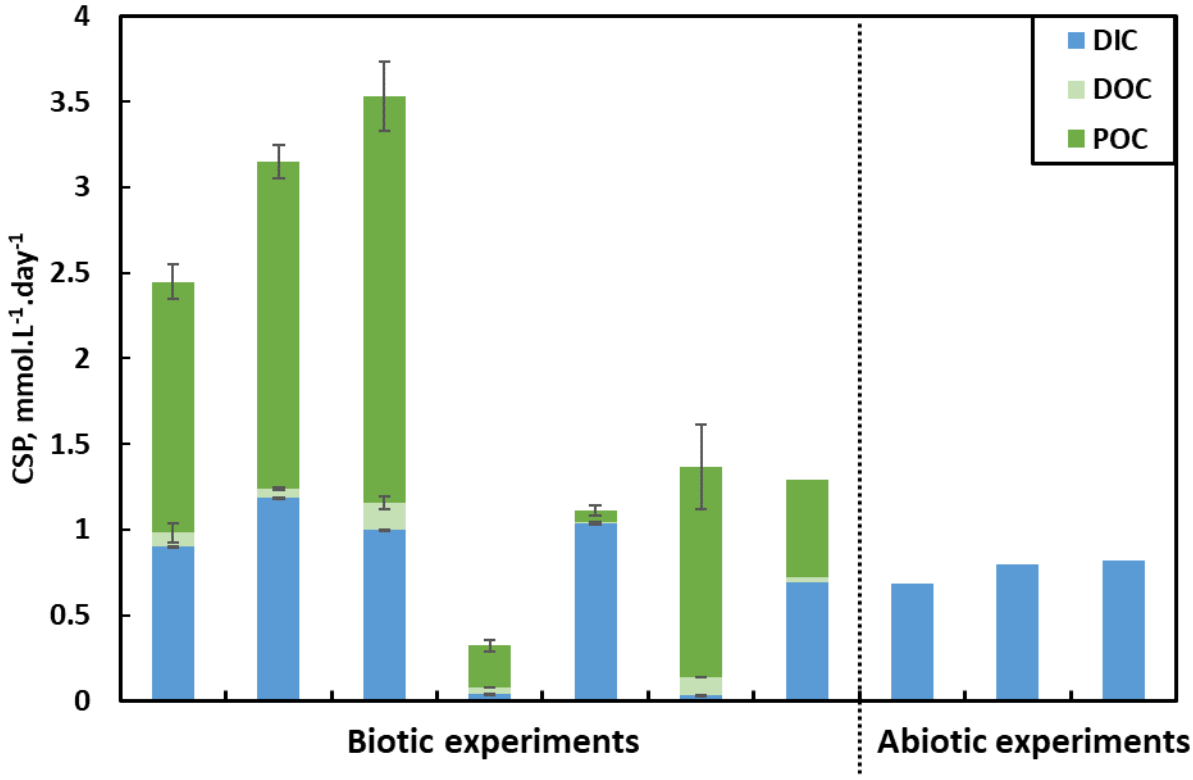

Figure 9. Comparison of carbon sequestration potential in biotic and abiotic experiments. Error bars represent standard deviation of replicates. Three forms of CO_2 sequestration – DIC, DOC and POC – represent mineral, soluble organic matter and cell biomass. See Table 1 for experimental conditions.